COMPRESSIVE RECONSTRUCTION FOR 3D INCOHERENT HOLOGRAPHIC MICROSCOPY

Oliver Cossairt[1], *Kuan He*[1], *Ruibo Shang*[1], *Nathan Matsuda*[1], *Manoj Sharma*[1], *Xiang Huang*[2], *Aggelos Katsaggelos*[1], *Leonidas Spinoulas*[1] *and Seunghwan Yoo*[1]

[1]Dept. of Electrical Eng. and Computer Science, Northwestern University, Evanston, IL 60208, USA
[2]Mathematics and Computer Science Division, Argonne National Laboratory, Lemont, IL 60439, USA

ABSTRACT

Incoherent holography has recently attracted significant research interest due to its flexibility for a wide variety of light sources. In this paper, we use compressive sensing to reconstruct a three-dimensional volumetric object from its two-dimensional Fresnel incoherent correlation hologram. We show how compressed sensing enables reconstruction without out-of-focus artifacts, when compared to conventional back-propagation recovery. Finally, we analyze the reconstruction guarantees of the proposed approach both numerically and theoretically and compare that with coherent holography.

Index Terms— Compressive sensing, incoherent holography, microscopy, inverse problems.

1. INTRODUCTION

Fresnel incoherent correlation holography (FINCH) [1] allows reconstruction of an unknown three-dimensional (3D) volume from its two-dimensional (2D) hologram under incoherent illumination. FINCH enables the extension of previously presented coherent holography reconstruction methods [2] to applications where incoherent light is present, such as white light or fluorescent imaging [3]. Moreover, it expedites the acquisition process compared to conventional imaging systems since it avoids scanning the 3D object in either space or time [4]. However, similar to coherent holography, FINCH suffers from out-of-focus artifacts when reconstructing a 3D scene using conventional back-propagation [1]. An ideal 3D reconstruction would "optically section" independent depth planes so that out-of-focus blur from one plane does not contaminate another. This, however, cannot be achieved with conventional back-propagation since it is a simple 2D-2D model linking the hologram plane to a single depth plane in the scene, while ignoring adjacent planes.

In this work, we show that compressed sensing (CS) can eliminate the out-of-focus artifacts of the FINCH system by exploiting sparsity of the 3D object in its native or a transformation domain. First, we analyze the 3D-2D forward model of the FINCH acquisition process. We then demonstrate the benefits of CS reconstruction [5,6,10] compared to traditional back-propagation [1]. Finally, following a similar approach to [7], we investigate the reconstruction guarantees of the proposed CS framework by means of the coherence parameter of the acquisition (or sensing) matrix of the FINCH system, and compare it to coherent holography systems. Our theoretical analysis gives greater insight into how the choice of FINCH system parameters affect 3D reconstruction performance.

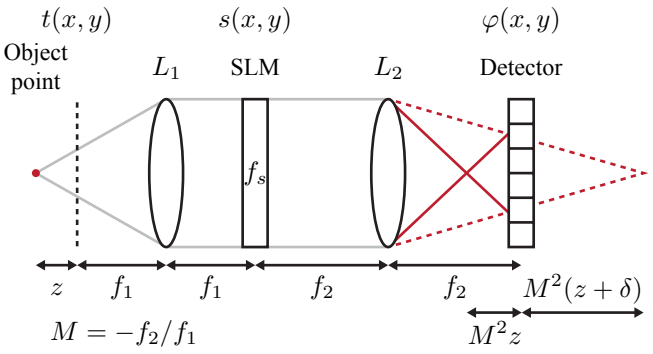

Fig. 1. A generalized diagram of a $4f$ FINCH system.

2. COMPRESSED SENSING FOR FINCH

2.1. Theory and model formulation

A FINCH system implemented using a $4f$ imaging system is illustrated in Figure 1. An object point at $(0,0,-z)$ with distance $z>0$ to the front focal plane of lens L_1 (i.e., input plane) produces a diverging spherical wave on the input plane,

$$t(x,y)=\frac{e^{ikz}}{i\lambda z}Q(z), \tag{1}$$

where λ is the central wavelength of the light, $k=2\pi/\lambda$ is the wavenumber, and $Q(z)=\exp\left[i\pi\left(x^2+y^2\right)/(\lambda z)\right]$ is the quadratic phase function. The complex field at the image plane of the $4f$ system can be described [1] as

$$\varphi(x,y)=\frac{e^{-i2k(f_1+f_2)}}{M\lambda^2f_2^2}t\left(\frac{x}{M},\frac{y}{M}\right)*\mathcal{F}\left\{s(x,y)\right\}\Big|_{\substack{f_x=x/(\lambda f_2),\\ f_y=y/(\lambda f_2)}}, \tag{2}$$

where $M = -f_2/f_1$ is the magnification factor, $*$ denotes 2D convolution and $\mathcal{F}$ is the 2D Fourier transform. The spatial light modulator (SLM) splits one object beam into two interfering beams, $s(x,y) = \left[1 + Q\left(-f_s\right)e^{i\theta}\right] \text{rect}\left(x/w, y/w\right)$, where θ is an adjustable phase constant and w is the width of the square-sized limited aperture of the $4f$ system [8]. Substituting Eq. (1) and $s(x,y)$ into Eq. (2), the hologram intensity at the sensor plane can be expressed as

$$|\varphi(x,y;z)|^2 = \frac{1}{M^2}\Big|\frac{e^{ikz}}{i\lambda z}Q\left(M^2 z\right) * f_c^2 sinc\left(f_c x, f_c y\right) + e^{i\theta}\frac{e^{ikz}}{i\lambda\left(z+\delta\right)}Q\left[M^2\left(z+\delta\right)\right] * f_c^2 sinc\left(f_c x, f_c y\right)\Big|^2, \quad (3)$$

where $\delta = f_1^2/f_s$ and $f_c = w/(\lambda f_2)$ is the optical cutoff frequency due to the limited aperture in the Fourier domain.

In order to eliminate the bias term and twin image from the hologram, we apply the phase-shifting technique [9] by recording three holograms with different values of θ, following Eq. (3). Using linear combinations of the three recorded holograms we obtain the final complex valued hologram, i.e., the point spread function (PSF) as

$$psf(x,y;z) = \frac{1}{M^2}\left[\frac{1}{i\lambda z}Q\left(M^2 z\right) * f_c^2 sinc\left(f_c x, f_c y\right)\right] \times \left\{\left[\frac{1}{i\lambda\left(z+\delta\right)}Q\left(M^2\left(z+\delta\right)\right)\right]^* * f_c^2 sinc\left(f_c x, f_c y\right)\right\}, \quad (4)$$

where * denotes the complex conjugate operator. As illustrated in Figure 1, the PSF can be interpreted as the multiplication of two spherical wave fields propagating for distances $M^2 z$ and $M^2(z+\delta)$, respectively. The quantity δ represents an axial shift between two spherical waves interfering on the sensor. This is a design parameter whose value may be controlled through the pattern displayed on the SLM. In the remainder of this paper we analyze the effect of δ on system performance.

The corresponding optical transfer function (OTF) can be calculated as the Fourier transform of the PSF as

$$OTF(f_x, f_y; z) = M^2\left[e^{-i\pi\lambda M^2 z\left(f_x^2+f_y^2\right)}\text{rect}\left(\frac{f_x}{f_c}, \frac{f_y}{f_c}\right)\right] * \left[e^{i\pi\lambda M^2(z+\delta)\left(f_x^2+f_y^2\right)}\text{rect}\left(\frac{f_x}{f_c}, \frac{f_y}{f_c}\right)\right]. \quad (5)$$

The final complex hologram $g(x,y)$ is given by the convolution between the complex PSF and the object intensity at different depths, subsequently integrated along the z axis. We assume that the 3D object, of size $L_x \times L_y \times L_z$, is placed with closest distance of z_0 to the left of the input plane. For digital reconstruction, we discretize the object into $N_x \times N_y \times N_z$ voxels of dimensions $\Delta_x \times \Delta_y \times \Delta_z$, where $\Delta_\xi = \frac{L_\xi}{N_\xi}$ for $\xi = \{x, y, z\}$. We simply choose the resolution N_x and N_y to match the sensor resolution, and $|M|\Delta_x \times |M|\Delta_y$ to match the sensor pixel size. Generally pixels have square size, thus we assume that $\Delta_x = \Delta_y = \Delta$. The depth resolution N_z is a user controlled parameter - as large as possible under desired reconstruction quality. The complex hologram $g(x,y)$ is sampled on a 2D pixel grid (x_u, y_v) as

$$g(x_u, y_v) \approx \sum_{r=1}^{N_z} psf\left(x_u, y_v; z_r\right) * f\left(x_u, y_v; z_r\right) = \sum_{r=1}^{N_z}\mathcal{F}^{-1}\left\{\mathcal{F}\left[psf(x_u, y_v; z_r)\right] \times \mathcal{F}\left[f(x_u, y_v; z_r)\right]\right\}, \quad (6)$$

where $1 \le u \le N_x, 1 \le v \le N_y$ and $z_r = z_0 + (r - 0.5)\Delta_z$.

Equation (6) can be expressed in matrix-vector form as

$$\mathbf{g} = \left[\mathbf{\Phi}_1, \ldots, \mathbf{\Phi}_{N_z}\right]\left[\mathbf{f}_1; \ldots; \mathbf{f}_{N_z}\right] = \mathbf{\Phi}\mathbf{f}, \quad (7)$$

where $\mathbf{f}, \mathbf{g}$ are the lexicographical representations of the 3D object voxels and the 2D sensed pixels, respectively, and

$$\mathbf{\Phi}_r \triangleq \mathbf{F^{-1}}\mathbf{D}_r\mathbf{F}, \quad (8)$$

where $\mathbf{D}_r$ is a diagonal matrix with diagonal elements corresponding to the lexicographical representation of the OTF at layer r.

It is clear from Eq. (7) that recovering a 3D volume $\mathbf{f}$ from its incoherent complex hologram $\mathbf{g}$ in FINCH is an ill-posed problem, because there are N_z times more unknowns than knowns. The newly developed CS theory [5, 6] suggests a way to solve the under-determined system by exploiting the sparsity of the unknown signal. CS reconstruction is usually formulated by solving the minimization problem

$$\min_{\mathbf{f}}\left\{\|\mathbf{g} - \mathbf{\Phi}\mathbf{f}\|_2^2 + \tau\|\mathbf{f}\|_1\right\}. \quad (9)$$

The first term in Eq. (9) measures the fidelity of a candidate estimate to the observed data. The second term calculates the ℓ_1 norm of the reconstructed signal and the regularization parameter $\tau > 0$ controls the ratio between the fidelity term and the level of sparsity of the object.

2.2. Simulation results

In this section, we demonstrate the benefits of CS reconstruction in FINCH when compared to conventional back-propagation. We assume the object consists of three thin layers placed at distances Δ_z , $2\Delta_z$, and $3\Delta_z$ from the input plane of the $4f$ system, respectively, with $\Delta_z = 3mm$. At each layer, the thin object has size $5.12mm \times 5.12mm$ and is discretized into 512×512 pixels of size $10\mu m \times 10\mu m$. We set $f_1 = f_2 = 0.25m$ and $f_s = 1m$, and compute $\delta = 62.5mm$ and generate the 2D hologram using the forward model of Eq. (7). We used both back-propagation from [1] and CS reconstruction modeled by Eq. (9) which was solved by employing the two-step iterative shrinkage/thresholding (TwIST) [11] algorithm.

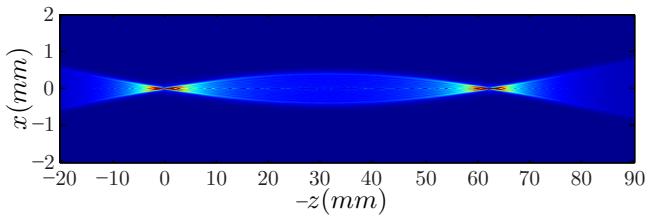

Fig. 2. The real part of the PSF in $x-z$ direction. The PSF is symmetric about $\delta/2$. The 3D object should be placed at $-z<0$ such that we operate on the left side of the figure.

Figure 2 depicts the PSF with the aforementioned parameters. The PSF's width along the x axis varies for different depths due to the limited physical aperture of the system. Figure 3 shows the reconstruction results for the simulated 3D scene. Figure 3(a) depicts the original object consisting of three different depth planes, while Figures 3(b) and 3(c) present reconstruction results using the standard back-propagation and the proposed CS approach, respectively. We can clearly see that each reconstructed plane by back-propagation (or refocusing) is distorted by out-of-focus artifacts (blurry images from adjacent depth planes), while CS provides better optical sectioning of the scene.

3. CS RECONSTRUCTION GUARANTEES

In this section, we investigate the performance of CS reconstruction for a $4f$ FINCH system by exploring the mutual coherence parameter of the system matrix. For simplicity, we assume that the object is sparse in the original space domain, so that the transform matrix is identity, and we only need to consider the coherence parameter of the sensing matrix $\mathbf{\Phi}$.

The coherence parameter μ can be computed as the maximal off-diagonal absolute value of the Gram matrix $\mathbf{G}=\tilde{\mathbf{\Phi}}^{\dagger}\tilde{\mathbf{\Phi}}$ [7, 12], where $\tilde{\mathbf{\Phi}}$ is column normalized, and $\dagger$ denotes the conjugate transpose operator. When the OTF has constant magnitude one, every $\mathbf{\Phi}_r=\mathbf{F^{-1}D}_r\mathbf{F}$ is column normalized, and the sub-Gram-matrix can be simplified as

$$\begin{aligned}\mathbf{G}_{k,l} &= \tilde{\mathbf{\Phi}}_k^{\dagger}\tilde{\mathbf{\Phi}}_l=\mathbf{\Phi}_k^{\dagger}\mathbf{\Phi}_l=\mathbf{F}^{-1}\mathbf{D}_k^{\dagger}\mathbf{F}\mathbf{F}^{-1}\mathbf{D}_l\mathbf{F}\\ &= \mathbf{F}^{-1}\mathbf{D}_k^{\dagger}\mathbf{D}_l\mathbf{F},(1\le k,l\le N_z)\,. \qquad (10)\end{aligned}$$

When the magnitude of the OTF is 1, $\mathbf{D}_k^{\dagger}\mathbf{D}_l$ and diagonal blocks $\mathbf{G}_{k,k}$ are indeed identity matrices (thus $\mathbf{\Phi}$ is column normalized). We only need to find the maximum absolute value of $\mathbf{G}_{k,l}$ for $k\neq l$. From [13], $\mathbf{G}_{k,l}$ is essentially a 2D convolution operator and has Toeplitz matrix form, whose entries are derived by convolution of two PSFs at layers k and l. Thus the coherence parameter is given by

$$\mu=\max_{\substack{1\le k,l\le N_z\\ k\neq l}}\max|\mathbf{G}_{k,l}|=\max_{\substack{1\le k,l\le N_z\\ k\neq l}}\max|psf_k*psf_l| \qquad (11)$$

The maximum number of the 3D points that can be guaranteed to be accurately reconstructed is given [7] by

$$S=0.5\,(1+1/\mu) \qquad (12)$$

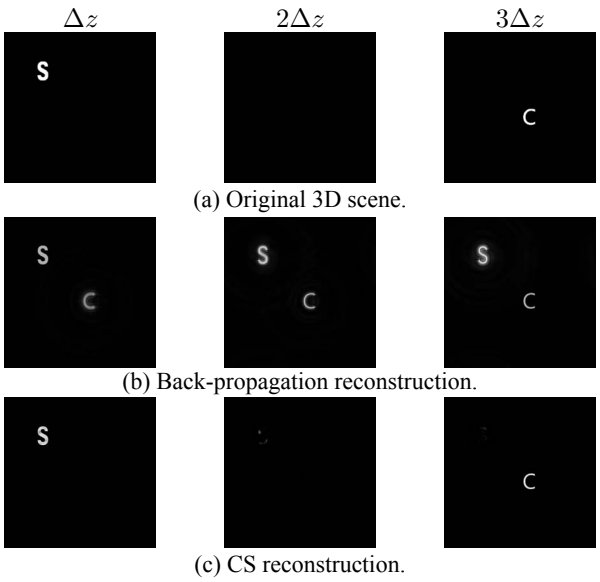

(a) Original 3D scene.

(b) Back-propagation reconstruction.

(c) CS reconstruction.

Fig. 3. Numerical experiment in FINCH: reconstruction of 3 different object depth planes of a 3D scene.

The result shown in Eq. (11) suggests that the coherence parameter is nothing but the maximum absolute value of correlation between any two PSFs. This corresponds to the correlation between two object points, which are located at two different depth planes. Based on this interpretation, one can predict according to Eq. (12) that by increasing the axial distance between two object points, the object features that can be accurately reconstructed by CS will also be increased.

Expanding the convolution in Eq. (5), we have

$$OTF\,(f_x,f_y;z)=M^2\Gamma(f_x;z)\Gamma(f_y;z)e^{-i\pi\lambda M^2\hat{z}\left(f_x^2+f_y^2\right)}, \qquad (13)$$

where $\hat{z}=z(z+\delta)/\delta=z+z^2/\delta$ and

$$\Gamma(f_x;z)=\int_{-\frac{f_c}{2}+\max(0,f_x)+\frac{M^2z}{\delta}f_x}^{\frac{f_c}{2}+\min(0,f_x)+\frac{M^2z}{\delta}f_x}e^{i\pi\lambda\delta t^2}dt. \qquad (14)$$

When f_c is large enough, $\Gamma(f_x;z)\Gamma(f_y;z)=\frac{i}{\lambda\delta}$ and

$$OTF\,(f_x,f_y;z)=\frac{iM^2}{\lambda\delta}e^{-i\pi\lambda M^2\hat{z}\left(f_x^2+f_y^2\right)}. \qquad (15)$$

For comparison, the OTF of the coherent holography system in [7] is given by

$$OTF_c\,(f_x,f_y;z)=e^{jkz}e^{-i\pi\lambda z\left(f_x^2+f_y^2\right)}. \qquad (16)$$

Since we need to scale the magnitude of OTF to 1, we could drop the $i\frac{M^2}{\lambda\delta}$ term in Eq. (15) when computing the coherence

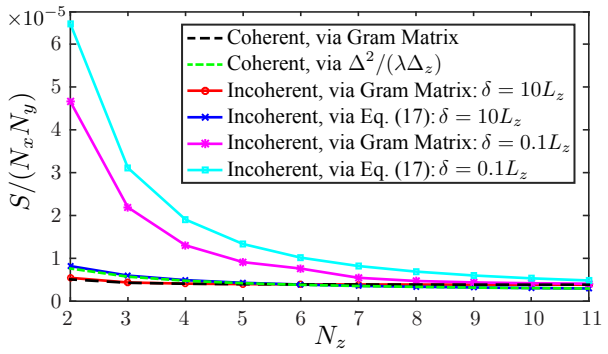

Fig. 4. Performance comparison of the FINCH system with coherent holography for different values of δ. The coherence parameter μ is computed both using the Gram matrix (through Eq. (11)) as well as directly through Eq. (17).

parameter. Moreover, since the e^{jkz} term in Eq. (16) gives rise to a $e^{jk(z_l - z_k)}$ term in $\mathbf{G}_{k,l}$, which has magnitude 1 and won't affect the coherence parameter, we could also drop e^{jkz} in our calculations. Further, when $|M| = 1$ and δ is much larger than z, $\hat{z} = z + \frac{z^2}{\delta} \approx z$, the proposed FINCH system yields the same performance as the coherent system [7].

The coherence parameter for the OTF of Eq. (16) depends on the closest z distance at different layers and can be derived as [7, 13] as $\mu_c \approx \frac{\Delta^2}{\lambda \min|z_k - z_l|} = \frac{\Delta^2}{\lambda \Delta_z}$. Similarly, the coherence parameter for the OTF of Eq. (15) depends on the closest $\hat{z}$ distance and can be derived as $\mu \approx \frac{\Delta^2}{\lambda M^2 \min|\hat{z}_k - \hat{z}_l|}$. Since $\min|\hat{z}_k - \hat{z}_l| = \Delta_z(1 + \frac{2(z_0+\Delta_z)}{\delta}) > \Delta_z$ (where z_0 is the closest distance from the object to the input plane of the $4f$ system), we have $\mu < \mu_c$ given $|M| = 1$, and our FINCH system yields less coherence and better performance than the coherent system, due to its more distinguishable OTFs at different layers. Formally,

$$\mu(\delta) \approx \frac{\Delta^2/(M^2\lambda\Delta_z)}{1 + \frac{2(z_0+\Delta_z)}{\delta}} = \frac{M^{-2}}{1 + \frac{2(z_0+\Delta_z)}{\delta}} \frac{L_x L_y}{\lambda L_z} \frac{N_z}{N_x N_y}, \quad (17)$$

$$S(\delta) \approx 0.5 + 0.5M^2 \left(1 + \frac{2(z_0 + \Delta_z)}{\delta}\right) \frac{\lambda L_z}{L_x L_y} \frac{N_x N_y}{N_z}. \quad (18)$$

In Figure 4, we show the performance of our FINCH system for large and small δ values and compare that with the coherent holography system in [7] given $z_0 = 0, M = -1$. We can see that our FINCH system has similar performance as the coherent system when δ is much larger than L_z, and much better performance for smaller δ.

We also demonstrate the limitation of CS reconstruction using the following numerical experiment: A 3D volume with constant length, $L_z = 1mm$, is generated, in which S identical point particles are randomly distributed. The number of the 3D volume pixels is $512 \times 512 \times N_z$, where $N_z = 2, \ldots, 10$ and $\Delta_x = \Delta_y = 10\mu m$. The object's 2D hologram is acquired by using the forward model of Eq. (7). As a solver, we use the TwIST algorithm [11] and limit the number

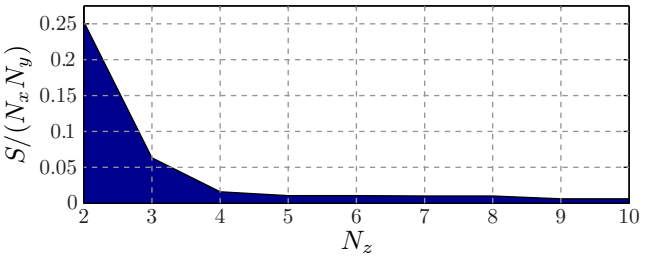

Fig. 5. Simulation results showing the normalized number of reconstructed 3D object's particles as a function of number of object planes, for a constant volume length, $L_z = 1mm$, given a sensor with 512×512 pixels.

of iterations to $10,000$. For each simulation instance with different N_z, the number of particles continues to increase until the mean squared error (MSE) between CS reconstruction and ground truth exceeds 10^{-5}. The results are shown in Figure 5. The shaded area denotes the region of acceptable 3D reconstruction (MSE $< 10^{-5}$) from the 2D incoherent hologram. Analyzing Figure 5, as z axial resolution becomes finer (or equivalently N_z become bigger for a constant volume length L_z), fewer 3D points can be reconstructed using CS, which is consistent with the theoretical predication of Eq. (18).

4. CONCLUSIONS AND FUTURE WORK

We have formulated the CS reconstruction of 3D objects from 2D incoherent holograms captured using a $4f$ FINCH system. We demonstrated that CS reconstruction can eliminate out-of-focus artifacts when compared with conventional back-propagation and analyzed its limitations both theoretically and numerically. Our analysis has given new insight into selection of FINCH system parameters. In particular, we have shown that some choices of FINCH system parameters result in better CS reconstruction performance than coherent Fresnel Holography [7]. While this observation warrants further investigation, it only represents a partial characterization of system performance. In particular, both our analysis and that of [7] ignores the effect of noise on system performance. However, the SNR of incoherent holography is known to be significantly worse than conventional holography due to the drastic reduction in fringe contrast. In future work, we plan on fully characterizing system performance by incorporating a detailed noise model into our CS analysis framework.

5. ACKNOWLEDGEMENTS

This work was supported in part by funding through the Biological Systems Science Division, Office of Biological and Environmental Research, Office of Science, U.S. Dept. of Energy, under Contract DE-AC02-06CH11357. The work was also supported in part by funding from NSF CAREER grant IIS-1453192 and ONR award N00014-15-1-2735.

6. REFERENCES

[1] Joseph Rosen and Gary Brooker, "Digital spatially incoherent Fresnel holography," *Opt. Lett.*, vol. 32, no. 8, pp. 912–914, Apr 2007.

[2] David J. Brady, Kerkil Choi, Daniel L. Marks, Ryoichi Horisaki, and Sehoon Lim, "Compressive holography," *Opt. Express*, vol. 17, no. 15, pp. 13040–13049, Jul 2009.

[3] Joseph Rosen and Gary Brooker, "Fluorescence incoherent color holography," *Opt. Express*, vol. 15, no. 5, pp. 2244–2250, Mar 2007.

[4] Joseph Rosen and Gary Brooker, "Non-scanning motionless fluorescence three-dimensional holographic microscopy," *Nat. Photonics*, vol. 2, no. 3, pp. 190–195, 2008.

[5] E. J. Candès, J. Romberg, and T. Tao, "Robust uncertainty principles: exact signal reconstruction from highly incomplete frequency information," *IEEE Trans. Inf. Theory*, vol. 52, no. 2, pp. 489–509, Feb 2006.

[6] E. J. Candès and M. B. Wakin, "An introduction to compressive sampling," *IEEE Signal Process. Mag.*, vol. 25, no. 2, pp. 21–30, March 2008.

[7] Yair Rivenson, Adrian Stern, and Joseph Rosen, "Reconstruction guarantees for compressive tomographic holography," *Optics letters*, vol. 38, no. 14, pp. 2509–2511, 2013.

[8] Ting-Chung Poon, *Optical Scanning Holography with MATLAB®*, Springer Science & Business Media, 2007.

[9] Ichirou Yamaguchi and Tong Zhang, "Phase-shifting digital holography," *Opt. Lett.*, vol. 22, no. 16, pp. 1268–1270, Aug 1997.

[10] Yair Rivenson, Adrian Stern, and Bahram Javidi, "Improved depth resolution by single-exposure in-line compressive holography," *Appl. Opt.*, vol. 52, no. 1, pp. A223–A231, Jan 2013.

[11] J. M. Bioucas-Dias and M. A. T. Figueiredo, "A new TwIST: Two-step iterative shrinkage/thresholding algorithms for image restoration," *IEEE Trans. Image Process.*, vol. 16, no. 12, pp. 2992–3004, Dec 2007.

[12] Alfred M. Bruckstein, David L. Donoho, and Michael Elad, "From sparse solutions of systems of equations to sparse modeling of signals and images," *SIAM Review*, vol. 51, no. 1, pp. 34–81, 2009.

[13] Yair Rivenson and Adrian Stern, "Conditions for practicing compressive Fresnel holography," *Opt. Lett.*, vol. 36, no. 17, pp. 3365–3367, Sep 2011.